Three-dimensional nanoconfinement of broadband optical energy in all-dielectric photonic nanostructure

Han Lin, Qiming Zhang, and Min Gu*

Centre for Micro-Photonics, Faculty of Engineering and Industrial Sciences, Swinburne University of Technology, Hawthorn VIC 3122, Australia
**Corresponding author: Mgu@swin.edu.au*

Received June 14, 2013; revised August 28, 2013; accepted August 28, 2013; posted August 29, 2013 (Doc. ID 192319); published September 30, 2013

We demonstrate the confinement of broadband optical energy in the visible to near-infrared regime in a three-dimensional nanoscale volume with high energy efficiency in a nanostructure consisting of multiple nanoslits in dielectric chacolgenide material. We find that a broadband optical field can be confined down to the scale of 1 nm ($\lambda/650$) with a confinement volume of $\lambda^3/3 \times 10^4$. The figure of merit of the nanostructure can be up to 10 times that achieved by plasmonic lensing and nanofocusing. Our work opens a new way for truly nanoscaled photonics applicable to nanolithograpy, nanoimaging, lab-on-chip nanosensing, single-molecule detection, and nanospectroscopy.

OCIS codes: (310.6628) Subwavelength structures, nanostructures; (350.4238) Nanophotonics and photonic crystals.

http://dx.doi.org/10.1364/PRJ.1.000136

1. INTRODUCTION

According to the conventional mechanism for focusing light, even for the vectorial theory for high numerical aperture (NA) objective lenses [1,2], the focal spot of an optical beam cannot be significantly smaller than its wavelength due to the diffraction nature of light. The figure of merit (FOM), defined as the ratio between energy confinement efficiency and effective confinement area [Eq. (4)], is depicted in Fig. 1(a) for a lens (black solid curve). Subwavelength imaging has been achieved in stimulated-emission-depletion (STED) microscopy [3]. This method is of great importance in nanoimaging, although nanoscale resolution is not achieved by the nanoconfinement of the illumination light energy. On the other hand, plasmonic lenses can focus surface plasmon polaritons (SPPs) in the near-field region with subwavelength resolution but have low energy confinement efficiency and thus a low FOM [Fig. 1(a)] [4–8]. Optical resolution and energy confinement can be improved through the use of the nanofocusing technique [9–13] to two-dimensionally (2D) confine the SPP energy between metallic components. This method, however, suffers from high optical loss due to the lossy nature of metal, in particular in the visible and near-infrared (NIR) regions. Furthermore, this method faces a great challenge set by the confinement-attenuation trade-off [14], which limits the FOM [Fig. 1(a)] of SPP nanofocusing even for well-fabricated structures. In addition, the narrow bandwidth of metal-based design prevents them from a range of applications requiring a broad spectrum such as nanospectroscopy [15]. Consequently, a fundamentally new photonic nanoconfinement scheme is needed for realizing highly efficient three-dimensional (3D) broadband optical confinement at a deep subwavelength scale without using metal.

In this paper, based on the dielectric chalcogenide glass (ChG) materials, we report on a tunable nanostructure capable of deep subwavelength confinement in three dimensions with high energy confinement efficiency up to 60% in the visible regime. The effective confinement area of the nanostructure can be concentrated to 3×10^3 times smaller than λ^2 of the incident beam [solid red curve in Fig. 1(a)], with an FOM several orders of magnitude higher than those of plasmonic lenses [4–8] and 10 times that of SPP nanofocusing [9–13]. Moreover, by tuning the refractive index of the ChG composition and photosensitivity [16,17], we can tune the enhancement peak from 520 to 760 nm while still maintaining strong energy confinement.

2. THEORETICAL MODELING

The 3D design of the dielectric nanostructure shown in Fig. 1(b) consists of three low-index ($n_s = 1$) nanoslits embedded in a high-index ($n_c = 2.5$) dielectric ChG block material, while the background material has a refractive index of $n_b = 1$. The ChG materials possess of a broad transmission wavelength window from the visible to NIR region [17]. In addition, ChG is sensitive to light illumination, whose index can be modulated by using light-induced phase change [16]. In this design, optical energy is confined in the central low-index nanoslit between the two high-index dielectric nanoridges [Fig. 1(b)]. The novelty of this geometry lies in that the photonic nanostructure uses an all-dielectric design to achieve optical energy confinement with higher energy confinement efficiency than the metal-based design. In addition, the finite-sized nanoslits also provide physical cavities for holding nanoparticles and single molecules in photochemistry experiments in an ultrasmall volume. Furthermore, the broadband

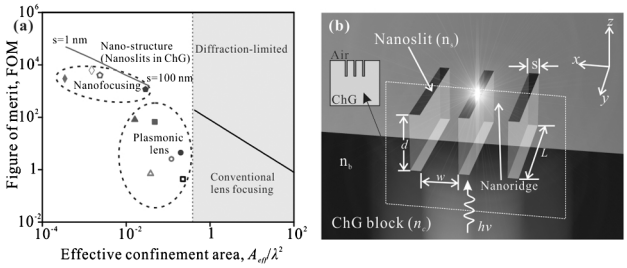

Fig. 1. (a) Plot of the FOM versus the effective confinement area enables a comparison of the nanostructure, optical lens focusing, plasmonic lenses (hollow square [4], solid square [5], hollow circle [6], solid circle [7], hollow triangle [8], solid triangle [8]) and nanofocusing (hollow pentagon [10], solid pentagon [11], hollow diamond [12], solid diamond [13]). The gray area marks the diffraction-limited. The curve of the FOM for the nanostructure is calculated when $d = 250$ nm and s varies in the range from 1 to 100 nm. (b) Schematic of the nanostructure. Three low-index nanoslits are embedded in the high-index ChG block. n_c is the refractive index of the ChG block, and n_s is the refractive index of the nanoslits. The refractive index of the background is n_b. L, s, and d are the length, width, and depth of the nanoslits, respectively. w is the width of the nanoridges. Inset: 2D cross section of the nanostructure.

property and the tunability of this design makes it an excellent platform for nanospectroscopic research.

In this study, the incident continuous-wave (CW) broadband optical plane waves polarizing in the x direction (TM mode) illuminate the nanostructure from the bottom. The wavelength range of the CW plane waves was from 0.5 to 1.5 μm in free space, and 400 discrete wavelength points were considered. The eigenmodes of the nanostructure can be formed due to the interaction between the eigenmodes within the individual nanoridges of width w and length L. Their values are selected to be $w = 140$ nm and $L = 500$ nm according to the experiment [18]. Then the width (s) and the depth (d) of the nanoslits are varied to study the effective confinement area A_{eff} [Eq. (1)] and effective confinement volume V_{eff} [Eq. (2)], the energy confinement efficiency η [Eq. (3)] and the FOM [Eq. (4)] at wavelength 650 nm according to the finite difference time domain (FDTD) method by using a commercial software package (Lumerical FDTD solutions [19]). Finally, the bandwidth and the tunability of the nanostructure are explored.

The effective confinement area A_{eff} is defined in the peak energy density plane normal to the beam propagation direction (x–y plane, light is propagating along the z direction) where $z = z_f$. Here we define A_{eff} as

$$A_{\text{eff}} = x_0 y_0, \tag{1}$$

where x_0 and y_0 are the full width at half-maximum (FWHM) for the energy density distribution along the x ($y = 0, z = z_f$) and y ($x = 0$, $z = z_f$) directions. The effective confinement volume V_{eff} is defined as

$$V_{\text{eff}} = x_0 y_0 z_0, \tag{2}$$

where z_0 is the FWHM of the energy density distribution along the z direction ($x = 0$, $y = 0$). A_{eff} and V_{eff} are normalized by λ^2 and λ^3. λ is the free space wavelength of the incident wave.

The energy confinement efficiency η is defined as the ratio of the total electromagnetic energy in effective confinement area A_{eff} in the peak energy density plane and the total incident electromagnetic energy in the incident plane where $z = z_{\text{in}}$:

$$\eta = \frac{\iint_{A_{\text{eff}}} W(x, y, z_f)\mathrm{d}x\mathrm{d}y}{\iint_{A_0} W(x, y, z_{\text{in}})\mathrm{d}x\mathrm{d}y}, \tag{3}$$

where $W(x, y, z) = (\varepsilon|E(x, y, z)|^2 + \mu_0|H(x, y, z)|^2)/2$ is the energy density and $A_0 = (500\ \text{nm})^2$ is the structure area of the nanostructure from the experiment [18]. As we use the uniform plane wave as the light source, $W(x, y, z_{\text{in}}) = W_0$ are equal across the incident plane, where W_0 is the energy density in the incident plane. Then we define the normalized energy density (enhancement) as $W(x, y, z)/W_0$.

To judge the performance of the light confinement (focusing) devices, we shall emphasize that both the effective confinement area and the energy confinement efficiency are important and related. Normally deep subwavelength confinement leads to low energy confinement efficiency. As indicated before, we describe this trade-off by a parameter called the FOM, which is defined as

$$\text{FOM} = \frac{\eta}{A_{\text{eff}}}. \tag{4}$$

This FOM characterizes the energy confinement efficiency under a given effective confinement area, which is a meaningful measure of the ability of confining light energy.

3. RESULTS AND DISCUSSION

The dependences of A_{eff}, η and FOM on s and d are shown in Figs. 2(a)–2(c). In the simulations, the domain size is 4 μm in the x and y directions and 6 μm in the z direction with a mesh grid of 0.1 nm, and the boundary condition is set to be a perfectly matched layer (PML). The mechanism for optical confinement in the nanostructure results from the mode coupling (coupling efficiency is 93%) [20,21], which depends on the depth of the nanoslits. The effective refractive index for the

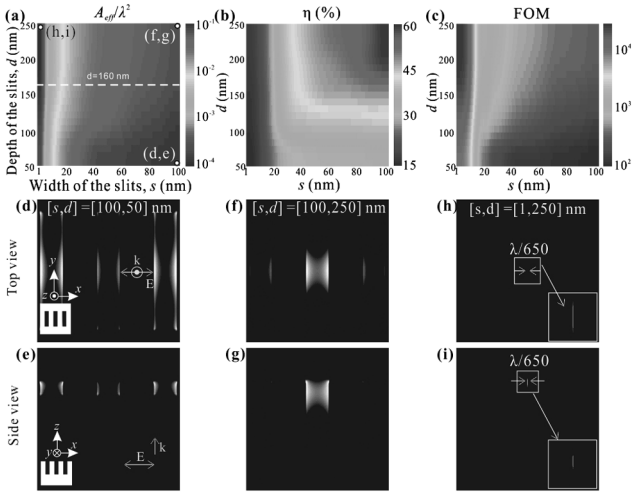

Fig. 2. Dependence of (a) effective confinement area A_{eff}, (b) energy confinement efficiency η, and (c) FOM of the mode on depth d and width s of the nanoslits. The white-dashed line marks the critical transformation length for mode coupling. (d)–(i) x–y and x–z cross sections of the energy density distribution of the nanostructures (d), (e) $[s, d] = [100, 50]$ nm, (f), (g) $[s, d] = [100, 250]$ nm, and (h), (i) $[s, d] = [1, 250]$ nm.

mode at 650 nm calculated by using a commercially available finite-element package from COMSOL [22] is 2.03, which results in an effective wavelength of 320 nm of the mode propagating in the nanoridges, corresponding to a critical transformation length of 160 nm (half of the effective wavelength) as marked by the white-dashed line in Fig. 2(a). When d is smaller than the critical transformation length (i.e., $d < 160$ nm) and s is large (e.g., $s = 100$ nm), the overall electric-field (E-field) distribution caused by the interference of the evanescent modes [Figs. 2(d) and 2(e)] cannot facilitate a small effective confinement area and a tight confinement of optical energy. To reduce the effective confinement area, a depth larger than the critical transformation length (i.e., $d > 160$ nm) is needed for efficiently coupling the propagation mode in the high-index nanoridges into the nanoslits. However, a large width of the nanoslits ($s = 100$ nm) still prevents the fields at the ChG–air interface in the central nanoslit from interacting with each other, as seen from the evanescent nature in the z direction [Figs. 2(f) and 2(g)]. When the nanosilt width reduces toward a deep subwavelength scale ($s = 1$ nm), the mode in the central nanoslit no longer shows the evanescent field shape. Instead, it is confined in three dimensions within the nanoslit [Figs. 2(h) and 2(i)] with the energy density enhancement up to two orders of magnitude and a moderate energy confinement efficiency of 17.5%, which is impossible for any metal-based nanofocusing design in which a SPP wave travels through a length of several wavelengths for deep subwavelength confinement [13].

The proportion of the mode energy residing within the nanoslit can be maximized up to 60% for $s = 100$ nm when $d = 250$ nm [Fig. 2(b)]. The strong energy confinement in the x–y plane in the nanoslit region occurs for two reasons. First, it arises from the continuity of the displacement field D at the material interfaces [21,22], which leads to a strong normal E-field component in the nanoslit. Second, in both nanoridges, the E-field components normal to the material interfaces are dominant, boosting the effect. Therefore, pure linearly polarized vectorial beams can be achieved in the central nanoslit, which can be quantified using the FOM. As shown by the red curve in Fig. 1(a), the FOM of the nanostructure can be up to 5×10^4, which is 10 times the best values of the nanofocusing design [12].

The energy confinement principle is further confirmed by resolving the E-field energy density in more detail. The field is confined between two high-index nanoridges [Fig. 3(a)] due to the E-field discontinuity in the x direction [21,22]. Meanwhile, the confinement in the y direction can be achieved simultaneously [Fig. 3(b)]. On the other hand, the confinement in the z direction is achieved [Fig. 3(c)] via the interference of light propagating in the positive z direction and the light reflecting at the ChG–air interface. The FWHM in the z direction increases as the depth of the nanoslits becomes large, accompanied with an enhancement in the E-field energy density. Figure 3(d) depicts the normalized effective confinement volume V_{eff} and the FWHM in the z direction as a function of s when $d = 250$ nm, showing the minimum value of 3.7×10^{-5} that occurs when the smallest FWHM (65 nm) is achieved, corresponding to the minimum effective confinement area.

To confirm its broadband nature, we look into the spectral property of the nanostructure. There are two broad enhancement peaks at wavelengths of 650 and 1140 nm in the spectral

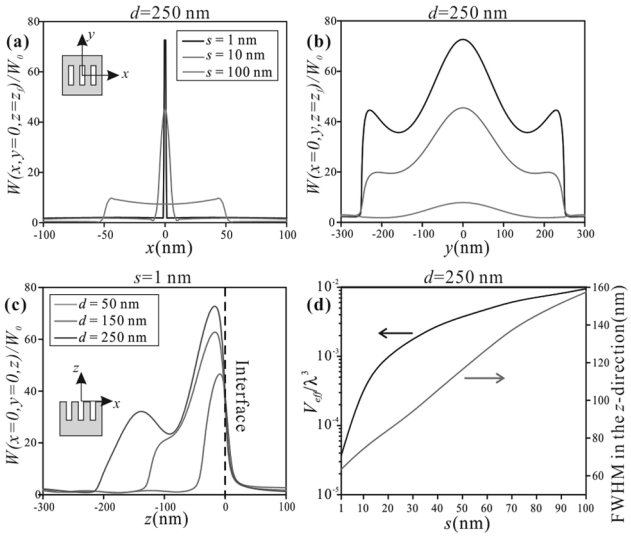

Fig. 3. Normalized energy density (a) along the x direction at $y = 0$, $z = z_f$ for the nanoslit with $d = 250$ nm, (b) along the y direction at $x = 0$, $z = z_f$ for the same d, and (c) along the z direction at $x = 0$, $y = 0$, for the nanoslits with a fixed $s = 1$ nm. The coordinates are marked in the figures. (d) Effective confinement volume V_{eff} and the FWHM in the z direction as a function of s when $d = 250$ nm.

range for $n_c = 2.5$ [Fig. 4(a)], and the mode in the nanoslits does not experience any significant cutoff within this region. Due to the broadband properties of the nanostructure, the calculated Q factor is approximately 1.5 in this case. For the wavelength shorter than 550 nm, strong confinement cannot be achieved because major parts of the optical energy are confined in the high-index nanoridges. For the wavelength longer than 1.4 μm, the modes are no longer be supported by the nanoridges.

The refractive index of the ChG block can be varied within a range of 2–3 by using different compositions [17] or light-induced phase change [16], which allows tuning of the enhancement and peak positions. As can be seen, the enhancement can be up to 100 as the index goes up to 3. The two enhancement peaks show the red shift with the increase of the refractive index, while the effective confinement area

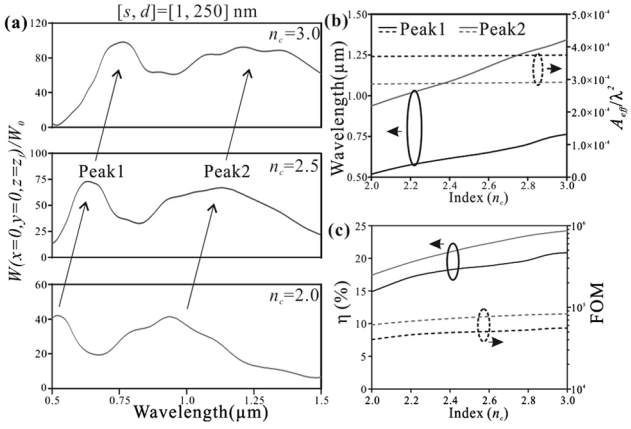

Fig. 4. (a) Spectral response of the nanostructure ($[s, d] = [1, 250]$ nm) with different n_c. Two enhancement peaks are shown in the curve. (b) Dependence of the enhancement peak wavelength (solid line) and A_{eff} (dashed line) on n_c for the two peaks. (c) Dependence of η (solid line) and the FOM (dashed line) on n_c for the two peaks.

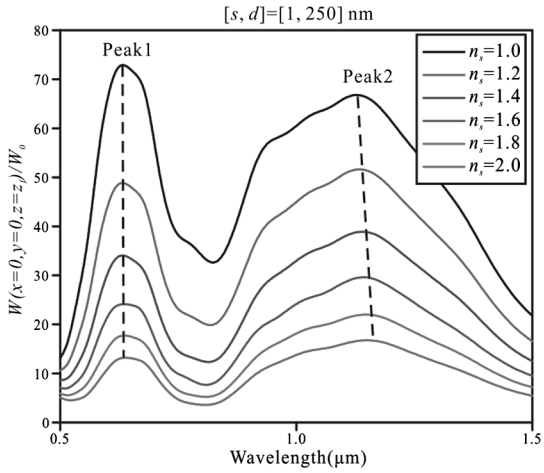

Fig. 5. Normalized energy density at the point of ($x = 0$, $y = 0$, $z = z_f$) versus the wavelength for different refractive indices of the nanoslits n_s ($[s, d] = [1,250]$ nm). The black-dashed lines mark the positions for two peaks for different values of n_s while $n_c = 2.5$, $n_b = 1$.

remains unchanged because the effective confinement area mainly depends on the geometry of the nanostructure. Meanwhile, the energy confinement efficiency becomes higher due to the stronger field enhancement in the nanoslit, which leads to an increase of the FOM. Define the tunability of the nanostructure as

$$t = \frac{\Delta\lambda}{\Delta n_c}, \tag{5}$$

where $\Delta\lambda$ is the wavelength shift, and Δnc is the change of the ChG index; we have $t_1 = 232 \pm 8$ nm/RIU for peak 1 and $t_2 = 409 \pm 3$ nm/RIU for peak 2. Another method for tuning the enhancement is to fill the nanoslits with other nanomaterials, which may be applicable in nanospectroscopy [15]. In this case, the enhancement of the two peaks of the nanostructure can be varied significantly while the position of the peaks remains almost unchanged (Fig. 5).

4. CONCLUSION

In summary, we have demonstrated an all-dielectric photonic nanostructure design for 3D deep subwavelength light confinement with high energy efficiency by using multiple nanoslits embedded in ChG block material, which is able to confine the optical energy in a 1 nm ($\lambda/650$) nanoslit to achieve an effective confinement area of $\lambda^2/3 \times 10^3$ with 17.5% energy confinement efficiency. The effective confinement area as well as the energy confinement efficiency and the FOM of the confined mode can be controlled by altering the width and the depth of the nanoslits. This approach is fully compatible with microlithography techniques and self-assembly methods [23] and laser-beam nanofabrication [18,24], which can be applied to nanoscale sensing and spectroscopy as well as single-molecule detection and near-field optical imaging with nanoscale illumination [25].

ACKNOWLEDGMENTS

This work is supported in part by the Australian Research Council (ARC) Centre for Ultrahigh-bandwidth Devices for Optical Systems (CUDOS) (Project No. CE110001018) as well as the Laureate Fellowship scheme (FL100100099).

REFERENCES

1. M. Gu, *Advanced Optical Imaging Theory* (Springer-Verlag, 2000), Chap. 6.
2. K. A. Serrels, E. Ramsay, R. J. Warburton, and D. T. Reid, "Nanoscale optical microscopy in the vectorial focusing regime," Nat. Photonics **2**, 311–314 (2008).
3. S. W. Hell and J. Wichmann, "Breaking the diffraction resolution limit by stimulated emission: stimulated-emission-depletion fluorescence microscopy," Opt. Lett. **19**, 780–782 (1994).
4. Z. Liu, J. M. Steele, W. Srituravanich, Y. Pikus, C. Sun, and X. Zhang, "Focusing surface plasmons with a plasmonic lens," Nano Lett. **5**, 1726–1729 (2005).
5. W. Srituravanich, L. Pan, Y. Wang, C. Sun, D. B. Bogy, and X. Zhang, "Flying plasmonic lens in the near field for high-speed nanolithography," Nat. Nanotechnol. **3**, 733–737 (2008).
6. W. Chen, D. C. Abeysinghe, R. L. Nelson, and Q. Zhan, "Plasmonic lens made of multiple concentric metallic rings under radially polarized illumination," Nano Lett. **9**, 4320–4325 (2009).
7. H. Shi and L. J. Guo, "Design of plasmonic near field plate at optical frequency," Appl. Phys. Lett. **96**, 141107 (2010).
8. L. Pan, Y. Park, Y. Xiong, E. Ulin-Avila, Y. Wang, L. Zeng, S. Xiong, J. Rho, C. Sun, D. B. Bogy, and X. Zhang, "Maskless plasmonic lithography at 22 nm resolution," Sci. Rep. **1**, 175 (2011).
9. D. K. Gramotnev and S. I. Bozhevolnyi, "Plasmonics beyond the diffraction limit," Nat. Photonics **4**, 83–91 (2010).
10. D. F. P. Pile and D. K. Gramotnev, "Adiabatic and nonadiabatic nanofocusing of plasmons by tapered gap plasmon waveguides," Appl. Phys. Lett. **89**, 041111 (2006).
11. H. Choi, D. F. P. Pile, S. Nam, G. Bartal, and X. Zhang, "Compressing surface plasmons for nano-scale optical focusing," Opt. Express, **17**, 7519–7524 (2009).
12. H. Choo, M. Stafarroni, T. J. Seok, J. Bokor, M. Wu, P. J. Schuck, S. Cabrini, and E. Yablonovitch, "Three-dimensional optical transformer—highly efficient nanofocusing device," in *Conference on Lasers and Electro-Optics and Quantum Electronics and Laser Science Conference* (IEEE, 2010).
13. M. Schnell, P. Alonso-González, L. Arzubiaga, F. Casanova, L. E. Hueso, A. Chuvilin, and R. Hillenbrand, "Nanofocusing of mid-infrared energy with tapered transmission lines," Nat. Photonics **5**, 283–287 (2011).
14. P. Berini, "Figures of merit for surface plasmon waveguides," Opt. Express **14**, 13030–13042 (2006).
15. S. Aksu, A. A. Yanik, R. Adato, A. Artar, M. Huang, and H. Altug, "High-throughput nanofabrication of infrared plasmonic nanoantenna arrays for vibrational nanospectroscopy," Nano Lett. **10**, 2511–2518 (2010).
16. T. Ohta, "Phase-change optical memory promotes the DVD optical disk," J. Optoelectron. Adv. Mater. **3**, 609–626 (2001).
17. A. Zakery and S. R. Elliott, "Optical properties and applications of chalcogenide glasses: a review," J. Non-Cryst. Solids **330**, 1–12 (2003).
18. Q. Zhang, H. Lin, B. Jia, L. Xu, and M. Gu, "Nanogratings and nanoholes fabricated by direct femtosecond laser writing in chalcogenide glasses," Opt. Express **18**, 6885–6890 (2010).
19. www.lumerical.com.
20. V. R. Almeida, Q. Xu, C. A. Barrios, and M. Lipson, "Guiding and confining light in void nanostructure," Opt. Lett. **29**, 1209–1211 (2004).
21. J. T. Robinson, C. Manolatou, L. Chen, and M. Lipson, "Ultrasmall mode volumes in dielectric optical microcavities," Phys. Rev. Lett. **95**, 143901 (2005).
22. www.comsol.com.
23. E. D. Mentovich, B. Belgorodsky, I. Kalifa, H. Cohen, and S. Richter, "Large-scale fabrication of 4-nm-channel vertical protein-based ambipolar transistors," Nano Lett. **9**, 1296–1300 (2009).
24. Z. Gan, Y. Cao, R. A. Evans, and M. Gu, "Three-dimensional deep sub-diffraction optical beam lithography with 9 nm feature size," Nat. Commun. **4**, 2061 (2013).
25. E. J. Sánchez, L. Novotny, and X. Sunney Xie, "Near-field fluorescence microscopy based on two-photon excitation with metal tips," Phys. Rev. Lett. **82**, 4014–4017 (1999).